Loss of Function of an RNA Polymerase III Subunit Leads to Impaired Maize Kernel Development[1][OPEN]

Hailiang Zhao,[a] Yao Qin,[1] Ziyi Xiao,[a] Qi Li,[b] Ning Yang,[c] Zhenyuan Pan,[a] Dianming Gong,[a] Qin Sun,[a] Fang Yang,[a] Zuxin Zhang,[a] Yongrui Wu,[b] Cao Xu,[c] and Fazhan Qiu[a,2,3]

[a]National Key Laboratory of Crop Genetic Improvement, Huazhong Agricultural University, Wuhan 430070, China

[b]National Key Laboratory of Plant Molecular Genetics, Chinese Academy of Science Center for Excellence in Molecular Plant Sciences, Institute of Plant Physiology & Ecology, Shanghai Institutes for Biological Sciences, Chinese Academy of Sciences, Shanghai 200032, China

[c]State Key Laboratory of Plant Genomics, National Center for Plant Gene Research, Institute of Genetics and Developmental Biology, The Innovative Academy of Seed Design, Chinese Academy of Sciences, Beijing 100101, China

ORCID IDs: 0000-0001-9093-711X (H.Z.); 0000-0001-5351-0459 (Q.L.); 0000-0001-8697-1681 (Z.Z.); 0000-0003-3822-0511 (Y.W.); 0000-0002-9055-7691 (C.X.); 0000-0002-0709-9635 (F.Q.).

Kernel size is an important factor determining grain yield. Although a number of genes affecting kernel development in maize (*Zea mays*) have been identified by analyzing kernel mutants, most of the corresponding mutants cannot be used in maize breeding programs due to low germination or incomplete seed development. Here, we characterized *small kernel7*, a recessive small-kernel mutant with a mutation in the gene encoding the second-largest subunit of RNA polymerase III (RNAPIII; *NRPC2*). A frame shift in *ZmNRPC2* leads to a premature stop codon, resulting in significantly reduced levels of transfer RNAs and 5S ribosomal RNA, which are transcribed by RNAPIII. Loss-of-function *nrpc2* mutants created by CRISPR/CAS9 showed significantly reduced kernel size due to altered endosperm cell size and number. ZmNRPC2 affects RNAPIII activity and the expression of genes involved in cell proliferation and endoreduplication to control kernel development via physically interacting with RNAPIII subunits RPC53 and AC40, transcription factor class C1 and Floury3. Notably, unlike the semidominant negative mutant *floury3*, which has defects in starchy endosperm, *small kernel7* only affects kernel size but not the composition of kernel storage proteins. Our findings provide novel insights into the molecular network underlying maize kernel size, which could facilitate the genetic improvement of maize in the future.

Increasing grain yield in maize (*Zea mays*) is required to meet the rapidly expanding demands for maize-derived foods, feed, and fuel. Kernel size, one of the most important factors determining grain yield, has been selected during maize domestication and improvement. Breeders enhance grain productivity in maize hybrids by pyramiding genes for desirable characteristics such as larger kernels. Maize kernel size is regulated by many factors, such as the supply of energy or material, cell proliferation and division, and important intracellular biological processes. To date, several defective kernel (*dek*) genes and empty pericarp genes have been cloned in maize. However, most of these genes encode pentatricopeptide repeat proteins and cannot be used in maize breeding programs due to incomplete seed development of the corresponding mutants (Xiu et al., 2016; Cai et al., 2017; Chen et al., 2017; Qi et al., 2017; Ren et al., 2017).

Unlike pentatricopeptide repeat proteins, *Dek44* encodes a mitochondrial ribosome protein that regulates maize kernel development by affecting the expression of chain-related proteins (Qi et al., 2019). *Dek15* encodes a homolog of SISTER CHROMATID COHESION PROTEIN4. The chromosome separation error in *dek15* results in reduced endosperm size and embryo lethality (He et al., 2019). The *varied kernel size1* mutant contains a mutation in *Zmkin11* that causes impaired spindle assembly, sister chromatid separation, and phragmoplast formation, leading to varying degrees of defective cell proliferation, ultimately resulting in the formation of seeds of different sizes (Huang et al., 2019).

[1]This work was supported by the National Key Research and Development Program of China (grant no. 2016YFD0101803) and the National Natural Science Foundation of China (grant nos. 31971951 and 31860382).

[2]Author for contact: qiufazhan@mail.hzau.edu.cn.

[3]Senior author.

The author responsible for distribution of materials integral to the findings presented in this article in accordance with the policy described in the Instructions for Authors (www.plantphysiol.org) is: Fazhan Qiu (qiufazhan@mail.hzau.edu.cn).

F.Q., Y.W., Z.Z., and H.Z. conceived the original screening and research plans; F.Q. supervised the experiments; H.Z., Y.Q., and Z.X. designed the experiments and analyzed the data; F.Q., Z.Z., F.Y., Y.W., C.X., and H.Z. drafted and critically revised the article; H.Z., Y.Q., Z.X., Q.L., N.Y., Z.P., D.G., and Q.S. performed the research.

[OPEN]Articles can be viewed without a subscription.

www.plantphysiol.org/cgi/doi/10.1104/pp.20.00502

The retinoblastoma-related (RBR) pathway controls maize endosperm development by regulating the cell cycle (Sabelli et al., 2013). Several important intracellular biological processes, such as post-transcriptional regulation, also play important roles in maize kernel development. These processes have been uncovered by studying mutants *rbm48* (Bai et al., 2019), *ubl1* (Li et al., 2017b), and *urb2* (Wang et al., 2018). These findings have enriched our knowledge of the regulatory mechanisms behind maize kernel development. However, most of these mutants exhibit significantly reduced kernel weight and defective seedling development, preventing them from producing normal offspring. Therefore, identifying and characterizing new genes controlling kernel size is still needed to provide genetic and molecular knowledge about kernel development that could be used to enhance breeding efforts for improving grain yield.

RNA polymerase III (RNAPIII) is the largest of the three eukaryotic RNA polymerases. The RNAPIII transcriptional complex consists of a 17-subunit enzyme and three transcription factors (TFIIIA, TFIIIB, and TFIIIC; Hoffmann et al., 2015; Abascal-Palacios et al., 2018). Early studies have shown that RNAPIII is responsible for the transcription of small noncoding RNAs, such as transfer RNAs (tRNAs), 5S ribosomal RNA (rRNA), U6 small nuclear RNA, and 7SL RNA (RN7SL1 RNA) in eukaryotes (Paule and White, 2000; Geiduschek and Kassavetis, 2001; Dieci et al., 2007). These small noncoding RNAs play widespread roles in basic biological activities, including protein synthesis (tRNAs), ribosome biogenesis (5S rRNA; Ciganda and Williams, 2011), mRNA splicing (U6 small nuclear RNA), membrane targeting of newly translated proteins (7SL RNA; Dieci et al., 2002), and selective mRNA export (SINE RNAs; Ponicsan et al., 2010; Karijolich et al., 2017) and they also act as cell-type–specific enhancers (*Alu* elements; Hardeland and Hurt, 2006; Zhang et al., 2019). These findings suggest that RNAPIII is required for growth, development, and reproduction (Goodfellow and White, 2007; Filer et al., 2017). However, most studies of RNAPIII subunit enzyme and transcription factors have been performed in yeast (*Saccharomyces cerevisiae*) and animals (Mann et al., 1992; Marshall and White, 2008; Pavon-Eternod et al., 2009), and few have focused on plants, especially studies involving RNAPIII subunits. In plants, a mutation of RNAPIII transcription-related plant AT-rich sequence and zinc binding protein suppressed the transcriptional activity of RNAPIII, leading to decreased grain length in rice (*Oryza sativa*) and floury endosperm in maize (Li et al., 2017c; Wang et al., 2019). Despite these findings, the components and mechanisms that regulate RNAPIII-mediated transcription and how the target genes transcribed by RNAPIII regulate endosperm development in plants have not been uncovered.

In this study, we characterized the maize *small kernal7* (*smk7*) mutant. This mutant has small kernels, good germination, good seedling development, and normal reproduction; small kernel size does not influence the grain yield or nutrition value of maize. We cloned *Smk7* and determined that it encodes the second-largest subunit of RNAPIII (NRPC2); *Smk7* is therefore referred to hereafter as *ZmNRPC2*. *smk7* contains a mutant version of *ZmNRPC2* that carries a frame shift and premature stop codon, resulting in small kernels due to impaired RNAPIII-mediated transcription. This mutation affects the transcription of genes involved in the mitotic cell cycle and DNA replication, which further inhibits cell proliferation and endoreduplication during endosperm development. Finally, we uncovered a regulatory pathway of *ZmNRPC2* and its effects on maize kernel development.

RESULTS

The *smk7* Mutant Produces Small Kernels

The *smk7* mutant was originally isolated from ethyl methanesulfonate-mutagenized Mo17 progeny (Fig. 1A). Compared with the wild type, mature *smk7* kernels were smaller, in terms of length, width, and thickness (Supplemental Fig. S1, A and B), and had a lower 100-kernel weight (~70% that of wild type), but no significant difference in the test weight (Fig. 1B). These differences made it easy to distinguish mutant *smk7* kernels from wild-type kernels by size, even on genetically segregating F1 ears as early as 8 d after pollination (DAP; Supplemental Fig. S2, B and C). The *smk7* kernels showed no germination defects and the resulting seedlings developed and reproduced normally, despite exhibiting weaker kernel growth than wild type (Supplemental Fig. S1, D and E).

Cytological observation revealed that fewer *smk7* endosperm cells stained positive for starch in *smk7* kernels than in wild-type kernels at different development stages, suggesting that they accumulated less starch, although *smk7* kernels produced normal endosperm and embryos (Fig. 1, C and D; Fig. S2C). The BETL cells in *smk7* kernels were smaller and lacked extensive cell wall ingrowths (Fig. 1, E and H). Moreover, the CZ cells were compacted lengthways (Fig. 1, E and F) and endosperm cells located in the area immediately internal to the AL were more similar to AL cells than endosperm cells, because they were smaller and accumulated less starch (Figs. 1, I and K). These results indicate that *smk7* is a small-kernel mutant with normal embryonic structures, but the cell shape in BETL, CZ, and peripheral of endosperm is different from wild type.

Loss of Function of *ZmNRPC2* Is Responsible for the Mutant Phenotypes

To identify the *Smk7* locus, the *smk7* mutant was crossed to the B73 inbred line and the progeny were selfed. The segregation ratio of wild-type to mutant

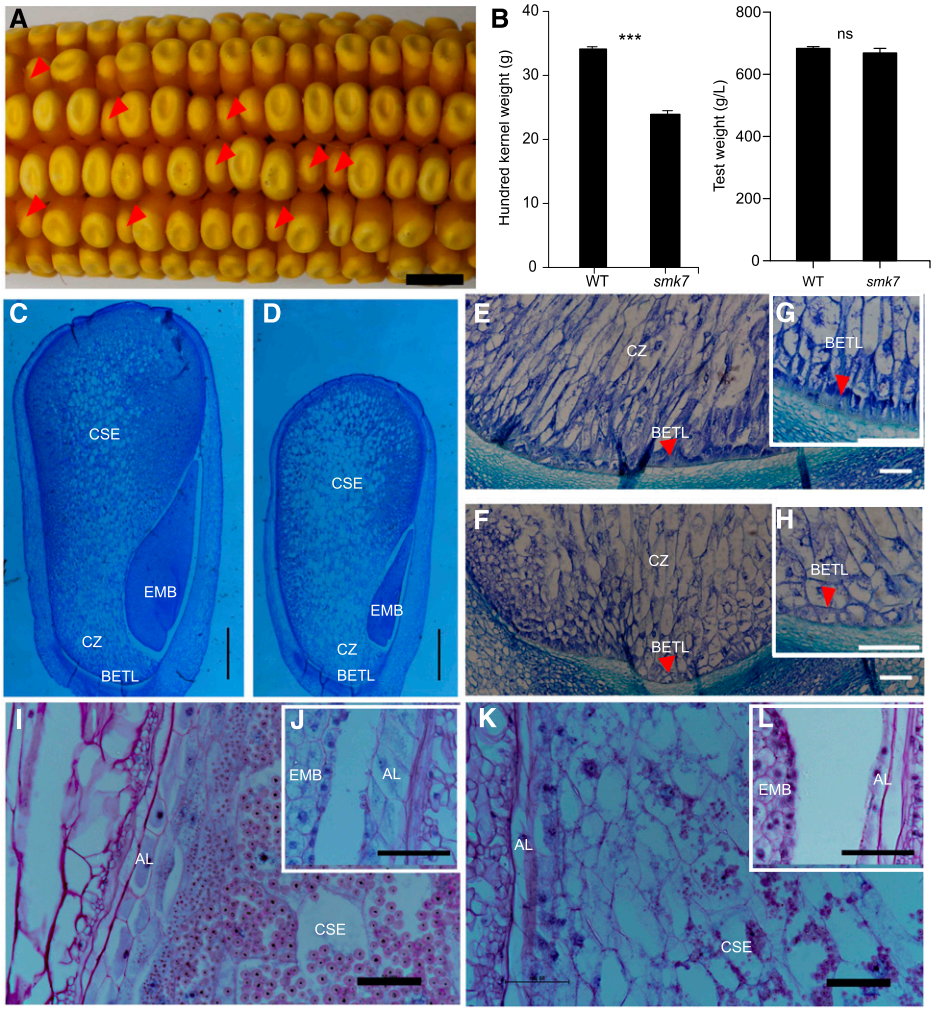

Figure 1. Phenotypic features of *smk7* kernels. A, Segregation of wild-type (WT) and *smk7* mutant kernels on an ear (arrow). Scale bar = 1 cm. B, Comparison of the 100-kernel weight (left) and test weight (right) of randomly selected mature wild-type and *smk7* kernels in a segregating F2 population. Values are means ± SE; $n = 3$. Asterisks indicate significant difference by Student's *t* test (***$P < 0.001$ and ns, $P > 0.05$). C and D, Longitudinal paraffin sections of developing wild-type kernels (C) and *smk7* kernels (D) at 15 DAP. E and F, Magnified basal endosperm transfer layer (BETL of wild-type kernels (E) and *smk7* kernels (F) at 15 DAP. G and H, Insets showing cell wall ingrowth of BETL cells in wild-type kernels (G) and *smk7* kernels (H) at 15 DAP. I and K, Magnified aleurone (AL) at peripheral regions of wild-type kernels (I) and *smk7* kernels (K) at 15 DAP. J and L, Magnified AL at embryo regions of wild-type kernels (J) and *smk7* kernels (L) at 15 DAP. CSE, Central starch endosperm; EMB, embryo; CZ, conducting zone; SA, Sub aleurone. Scale bars = 1,000 μm (C and D) and 100 μm (E–L).

kernels on the self-crossed ears was 1,477:490, which is ~3:1 (χ^2-test, $P > 0.05$), indicating that the *smk7* mutant is a monogenic recessive mutation (Supplemental Fig. S2A). Bulk-sequence analysis was then performed and the *smk7* was mapped to a 63.64-Mb interval on chromosome 6 (from 19,352,816 to 83,002,397 bp; Fig. 2A). Using 4,300 mutant individuals, *smk7* was fine-mapped to a 2.61-Mb region (from 61,269,234 to 63,875,645 bp) that was flanked by two developed insertion/deletion markers (ID51 and ID76; Fig. 2B). The 2.61-Mb mapping interval contained 22 genes that were annotated on the B73 reference genome version 4 (B73 RefGen V4; Jiao et al., 2017). Among these, a G-to-T substitution located at the splice acceptor in the 36th exon of *Zm00001d035960* was detected and confirmed (Fig. 2C). This G/T mutation resulted in an alternatively spliced transcript that retained a 26-bp intron, which caused a frame-shift that generated a premature stop codon. The alternatively spliced transcript can be translated to generate a protein lacking three amino acids and containing 13 changed amino acids. We estimated the expression of *Zm00001d035960* transcripts and observed that the alternatively spliced transcript accounted for 75% of the total mRNA, suggesting the *smk7* mutant phenotype might be attributed to a decrease in wild-type transcripts of *Zm00001d035960* (Fig. 2D).

The Zm00001d035960 protein showed high sequence similarity to the DNA-directed RNAPIII subunit 2 (NRPC2) of well-studied species such as *Homo sapiens*, *Mus musculus*, and *S. cerevisiae* (Supplemental File S1); thus, it is hereafter referred to as *ZmNRPC2*. Phylogenetic analysis showed that *ZmNRPC2* clustered within the monocot *NRPC2* clade (Fig. 3A). The defective protein from the alternative transcript showed a loss of the conserved RNA_pol_Rpb2_7 domain, which contains a region termed "switch 4" (Fig. 3B; Supplemental Fig. S3A). The switch domains within the polymerase are thought to signal different stages of transcription (Cramer et al., 2001) and interact with the "clamp domain" of NRPC1 (Supplemental Fig. S3C; Cramer et al., 2001). The alternative smk7 protein also lacked an α-helix and a β-folding domain (Supplemental Fig. S3B), which formed 14 hydrogen bonds in the predicted three-dimensional structure (Supplemental Fig. S3D), suggesting that a defective ZmNRPC2 protein was present in the *smk7* mutant.

We further examined the expression pattern of the *ZmNRPC2* gene via reverse transcription quantitative

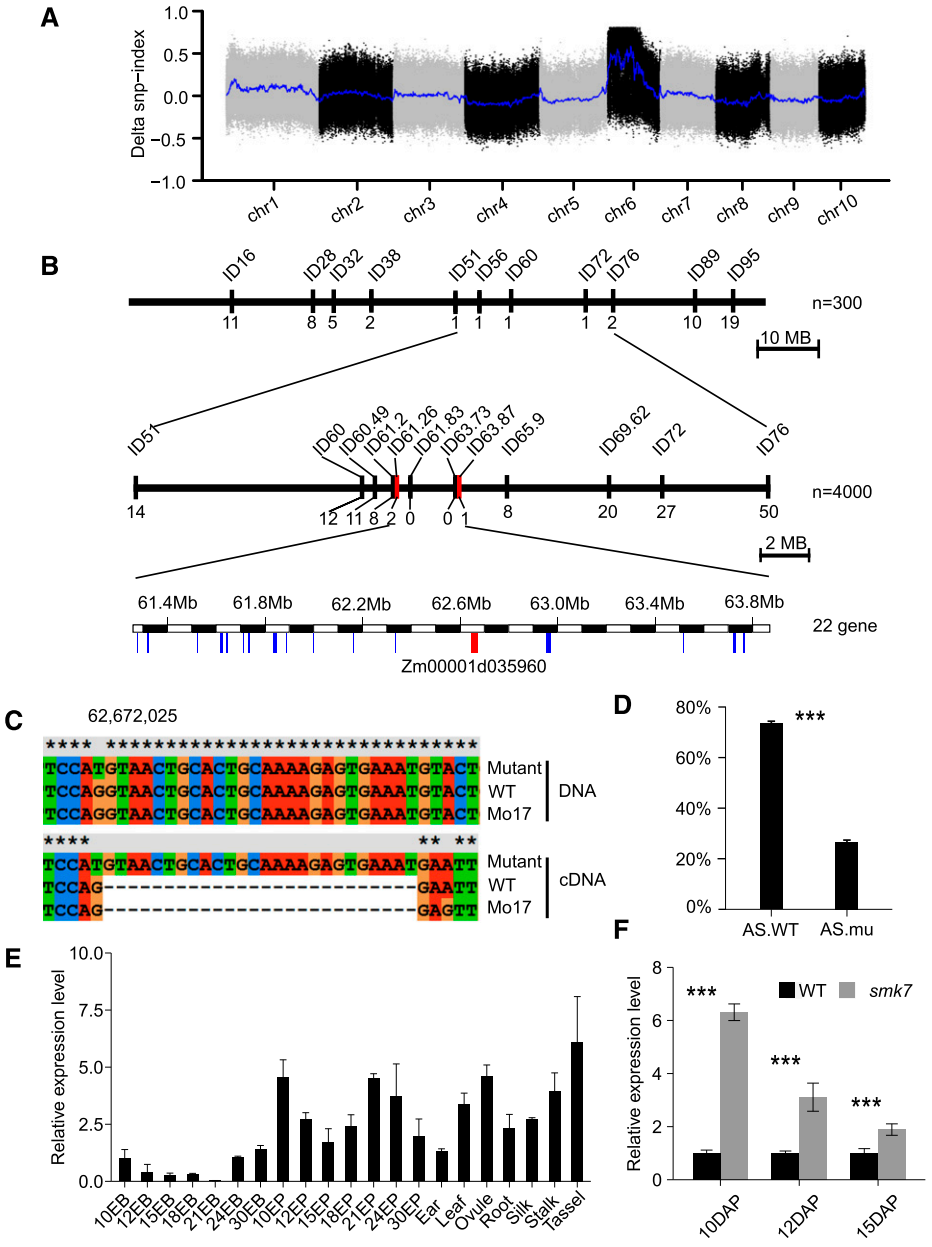

Figure 2. Positional cloning and identification of *smk7*. A, Mapping by sequencing of *smk7* gene, Delta-SNP index between mutant and wild-type (WT) pools of segregating phenotypic classes. Black and gray points in the graphs represent SNPs in different chromosomes, and the blue line represent the sliding window average of 500 SNPs interval with 50 SNPs increment. B, The *smk7* gene locus was mapped to a 2.61-Mb region on chromosome 6 with 22 candidate genes. The red lines represent *ZmNRPC2*; the blue lines represent other genes in the interval between marker ID61.26 to ID63.87. C, The mutation site of the *Zm00001d035960* gene. D, Analysis of the proportion of mutant cDNA in *smk7* using monoclonal methods. Values are means ± SE. $n = 3$. Asterisks indicate significant difference by Student's *t* test (***$P < 0.001$). E, RT-qPCR analysis of *ZmNRPC2* in various tissues and in developing kernels. F, Comparison of the expression level of *ZmNRPC2* in wild-type and mutant endosperm at 10, 12, and 15 DAP. Values are means ± SE. $n = 4$. Asterisks indicate significant difference by Student's *t* test (***$P < 0.001$).

PCR (RT-qPCR), which showed that it was constitutively expressed in diverse wild-type maize tissues (Fig. 2E), with a relatively high expression level in the tassel and ovule. The level of the *ZmNRPC2* expression decreased throughout endosperm development from 10 to 15 DAP, increased from 15 to 21 DAP, and then gradually decreased. To investigate the effect of the *nrpc2* mutation, we examined the *ZmNRPC2* transcript level in immature endosperm of wild type and *smk7* at 10, 12, and 15 DAP by RT-qPCR analysis (Fig. 2F). Surprisingly, an increased level of *ZmNRPC2* transcripts was detected at these three developmental stages in the *smk7* mutant.

To identify the function of *ZmNRPC2* in maize kernel development, we generated three independent *ZmNRPC2* knock-out transgenic lines that contained either a 901-bp deletion including the first to the third exons of *ZmNRPC2* (*nrpc2-KO1*), a 1-bp deletion in the 36th exon =(*nrpc2-KO2*), or two single-nucleotide polymorphisms (SNPs) in the 36th exon (*nrpc2-KO3*; Fig. 4A). The self-crossed ears of heterozygous plants showed a segregation in kernel size, with 161 wild-type:63 mutant kernels in *nrpc2-KO2*/+ and 186 wild-type:68 mutant kernels in *nrpc2-KO3*/+, which was not statistically significantly different from a 3:1 segregation ratio (χ2-test, $P > 0.05$; Fig. 4B). In the self-crossed ears of *nrpc2-KO1*/+, homozygous s mutant kernels were developmentally arrested, with blocks in embryogenesis and endospermogenesis (Fig. 4B), which might be explained by the *zmnrpc2* mutation that caused a deletion within the protein. The *nrpc2-KO2* and *nrpc2-KO3* mutated proteins were generated by mutations within the 36th exon of *ZmNRPC2*, which

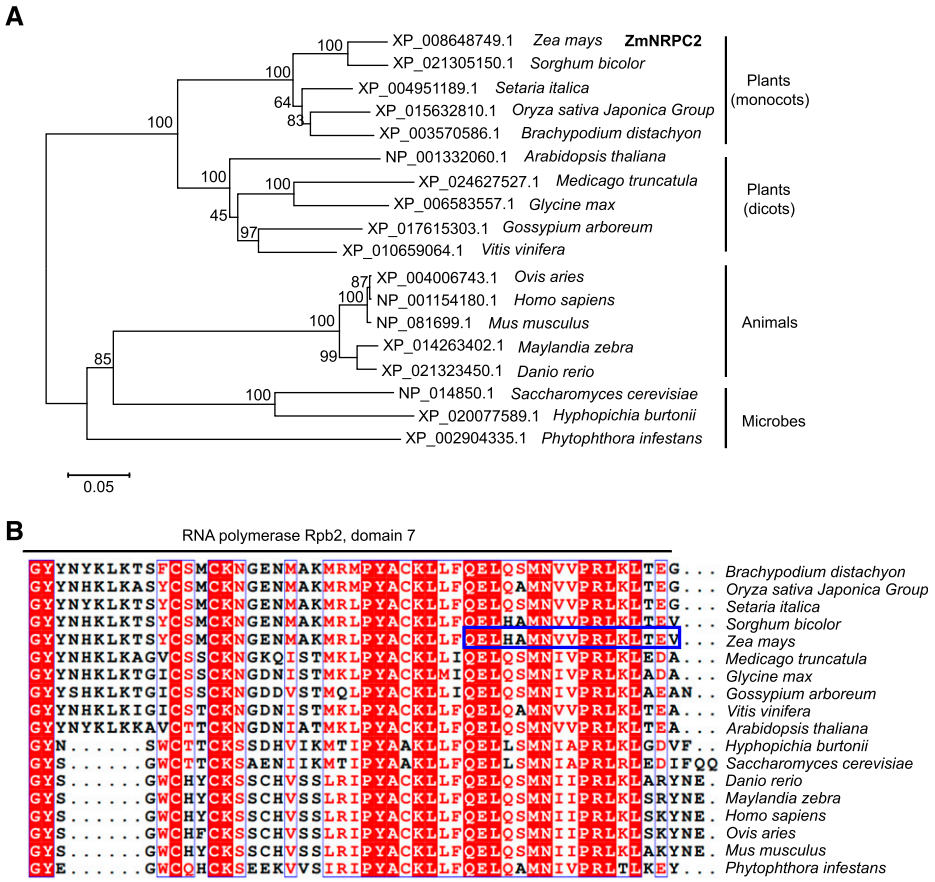

Figure 3. Phylogenetic analysis of NRPC2. A, Neighbor-joining sequence similarity analysis of ZmNRPC2 and its homologs in other organisms. The phylogenetic reconstruction was conducted in the program MEGA7.0 (https://www.megasoftware.net/). The numbers next to the branches represent the percentage support from 1,000 bootstraps. Scale bar = mean number of amino acid substitutions per site. B, The RNA_pol_Rpb2_7 domain in NRPC2 is conserved. If the score is greater than global score of similarity, it will be rendered as colored characters (red characters on a white background by default and red characters on a red background if residues are strictly conserved in the column) with blue frames. Bold blue frame in *Z. mays* represent mutation residues.

created two weaker alleles of *zmnrpc2*. These results indicated that *ZmNRPC2* is required for kernel development in maize (Figs. 1A and 4B). Allelism tests were performed by crossing three independent heterozygous mutated alleles with *smk7*. The hybrid ears showed defective phenotypes similar to those obtained by self-crossing *nrpc2-KO1*/+, *nrpc2-KO2*/+, and *nrpc2-KO3*/+ ears (Supplemental Fig. S4), indicating that *ZmNRPC2* is the mutated gene in *smk7*.

ZmNRPC2 Interacts with Subunits of the RNAPIII Complex and Regulates Expression of tRNAs and 5S rRNA

A search of the maize protein database via BLASTP (https://blast.ncbi.nlm.nih.gov/Blast.cgi?PROGRAM=blastp&PAGE_TYPE=BlastSearch&LINK_LOC=blasthome) with sequences of subunits of the RNAPIII complex of *S. cerevisiae* and *H. sapiens* identified the amino acid sequences of maize RNAPIII subunits. The full-length open reading frames (ORFs) of subunit-encoding genes were constructed into pGADK7 and the full-length ORF of *ZmNRPC2* and *dNRPC2* (defective *ZmNRPC2*, representing the mutation in *smk7*) were separately cloned into pGBKT7. The yeast two-hybrid (Y2H) assay and bimolecular luciferase complementation (BiLC) assays revealed that RNAPIII complex subunits, including RPC53, the AC40, and the TFIIIC subunit TFC1, and the key FL3 protein in endosperm development, physically interacted with ZmNRPC2 and dNRPC2 (Fig. 5, A and B), indicating that ZmNRPC2 is important for the function of the RNAPIII transcription complex. Furthermore, ZmNRPC2 and dNRPC2 were localized to the cytoplasm and the nucleus (Supplemental Fig. S5), and the G/T mutation in *smk7* did not affect their subcellular localization. These results indicated that the peptide that was absent from the mutant Smk7 protein was not essential for protein–protein interaction, and suggest that dNRPC2 competitively binds with subunits of the RNAPIII complex to counteract ZmNRPC2 function in vivo.

To elucidate the effects of ZmNRPC2 on transcription, we analyzed the biogenesis of tRNAs and 5S rRNA and observed that the transcript levels of 5S rRNAs and 17 tRNAs were more than 2-fold lower in *smk7* endosperm cells than in wild type; in particular, the expression of four tRNAs (tRNA-Trp, tRNA-Pro, tRNA-Arg, and tRNA-Gly) was reduced by more than 10-fold relative to that in wild-type endosperm cells (Fig. 5C), suggesting that ZmNRPC2 regulates the transcription of 5S rRNAs and tRNAs in kernel endosperm cells.

ZmNRPC2 Genetically Interacts with *FL3*

To test the interaction between ZmNRPC2 and FL3, we crossed *smk7* to *fl3* and identified single and double

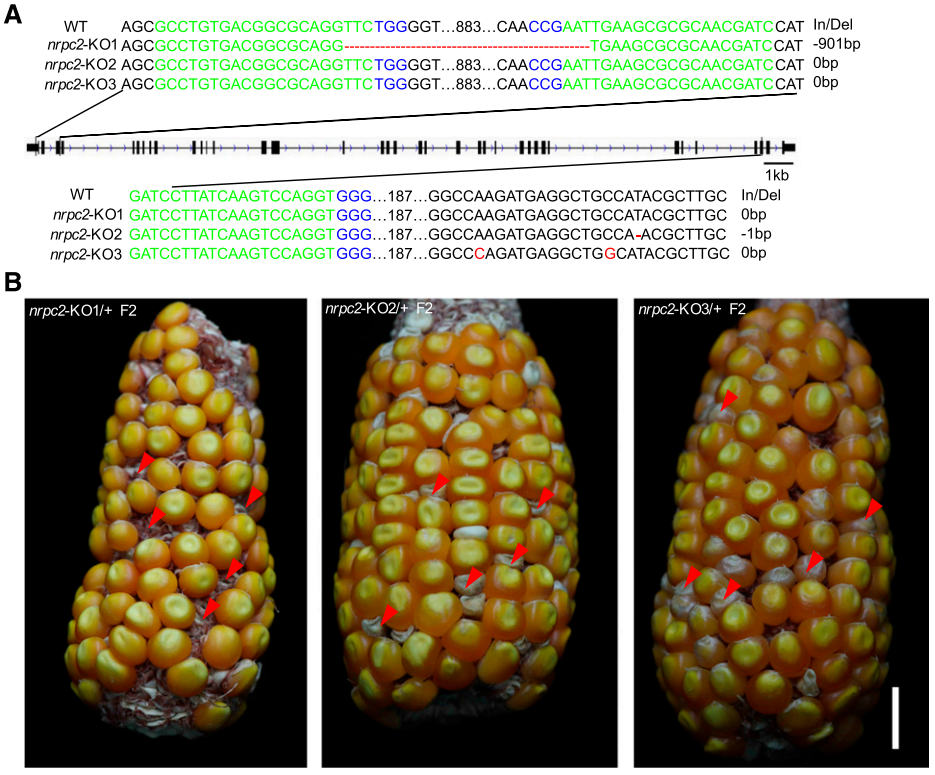

Figure 4. CRISPR-Cas9–based mutation of *Smk7*. A, The sequence within the *Zm00001d035960* locus was targeted using CRISPR/Cas9. The guide RNA target sequence and the protospacer-adjacent motif are shown in green and blue, respectively. Alignments of the mutant sequences from three independent transgenic plants are indicated. Red letters and dashes represent SNPs and deletions, respectively. WT, Wild type. B, Mature F2 ear of *nrpc2-KO1*/+, *nrpc2-KO2*/+, and *nrpc2-KO3*/+. Arrows indicate defective kernels. Scale bar = 2 cm.

mutant kernels on self-crossed F1 ears by genotyping. We observed an opaque and soft endosperm phenotype for *fl3* kernels, which differed from the small-kernel phenotype of *smk7*; the double *smk7;fl3* mutant exhibited cumulative features of the two single mutants and possessed small and opaque kernels (Figs. 6A and 7A). The 100-kernel weight of *smk7* and the *fl3* was 47.5% and 54.2% lower, respectively, whereas the 100-kernel weight of the double mutants was even lower (76.2%) relative to that of wild type (Fig. 6B), suggesting that the effect of both *smk7* and *fl3* on kernel weight was cumulative.

Consistent with the decreased kernel weight phenotype, the size of the endosperm of *smk7* and *smk7;fl3* kernels was dramatically reduced by 47.2% and 60%, respectively, at 10 DAP (Supplemental Fig. S6D), and decreased by 26.9% and 48.3% in 15 DAP kernels, respectively, relative to wild type (Fig. 6D). However, the endosperm of *fl3* was 10.9% smaller than that in wild-type kernels (Fig. 6D), showing a difference in endosperm size between *fl3* and *smk7* and genetic additivity in *smk7;fl3*. To compensate for reduced endosperm size, the endosperm cells of *fl3*, *nrpc2*, and *nrpc2;fl3* were significantly larger than those in wild type (Fig. 6, E and F; Supplemental Fig. S6D), demonstrating that the number of endosperm cells is dramatically decreased in all three mutants. The difference between *fl3* and *smk7;fl3* might be due to higher compensatory expression of *ZmNRPC2* in *fl3* (Fig. 6C). Transmission electron microscopy revealed that the number and size of starch granules and protein bodies in the endosperm of the three mutants were drastically smaller than that in wild type (Fig. 6, G and H). This indicates that the reduced kernel size of the three mutants is associated with the repression of cell proliferation and storage reserve filling.

The opaque and soft endosperm phenotype of *fl3* kernels (Li et al., 2017c) was not observed in the *smk7* mutant and the *nrpc2-KO* lines. To identify the basis for this difference in endosperm phenotype between *fl3* and the *smk7*, we tested the content of starch and storage proteins in the dry powder of mature kernels. The starch content did not differ significantly among the three mutants (Supplemental Fig. S6C). Compared with wild-type kernels, the levels of zeins in kernels of *fl3* and *smk7;fl3* were 23.8% and 24.4% lower than those in wild type, respectively, whereas the level of nonzein proteins significantly increased by 56.4% and 109.7%, respectively (Fig. 7D). However, the levels of zeins and nonzein proteins did not differ significantly between *smk7* and wild type (Fig. 7D). Similarly, the levels of most free amino acids showed no significant difference among the mutants, except for Arg, Lys, and Met, which were slightly less abundant in *smk7* kernels than in wild-type kernels. Notably, the levels of free amino acids dramatically increased in *fl3* and *smk7;fl3* kernels (Fig. 7E). Scanning electron microscopy revealed that the starch granules in the endosperm were tightly embedded within the storage protein body matrix in wild-type and *smk7* kernels, but were naked in *fl3* and *smk7;fl3* (Fig. 7, B and C). These results demonstrate that the ratio of zeins/nonzeins was altered in *fl3* kernels but not in *smk7*.

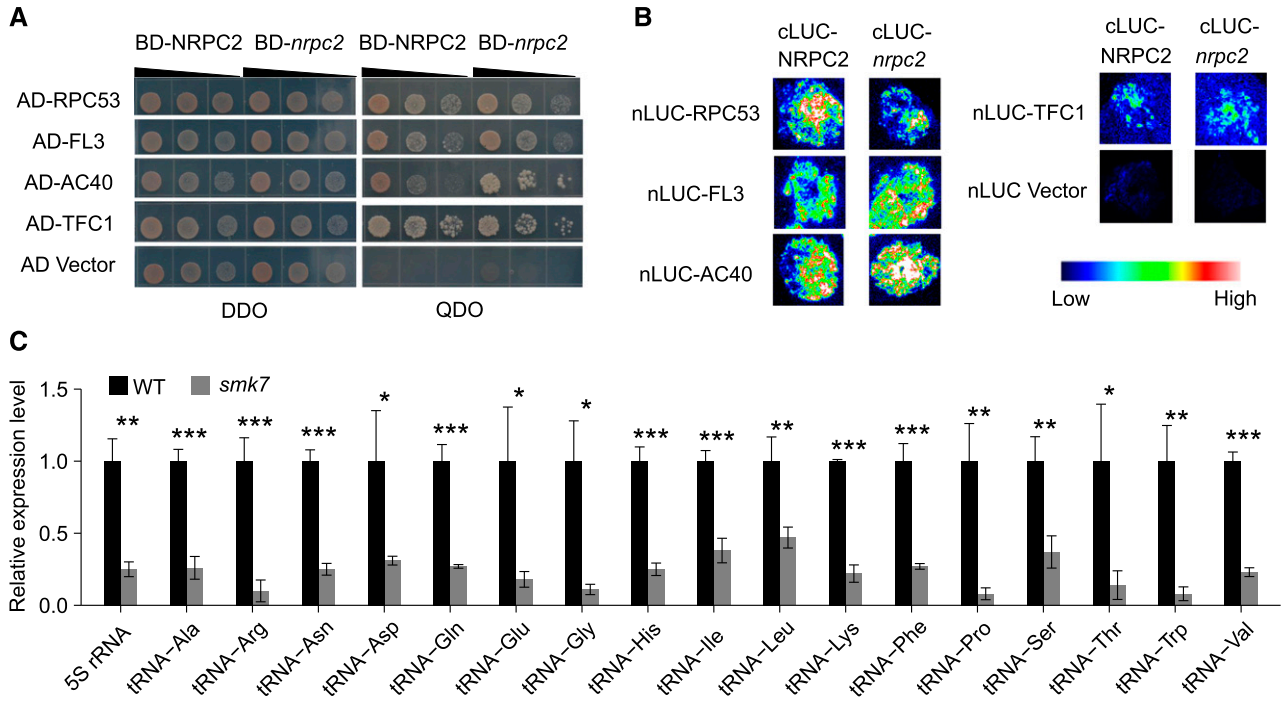

Figure 5. Analysis of the interaction between ZmNRPC2 and RNAPIII and FL3, and expression of 17 tRNAs and 5S rRNA in wild type (WT) and *smk7* endosperms at 15-DAP. ZmNRPC2 interacts with key factors of the RNAPIII transcription machinery and restricts RNAPIII transcription activity. A, Y2H assay showing that ZmNRPC2 and dNRPC2 interact with RPC53, AC40, TFC1, and FL3. The yeast cultures with three different dilutions (10, 10^{-1}, and 10^{-2}) were grown on the SD medium lacking Trp, Leu, His, and Ade (right) and lacking Trp and Leu (left, as control), respectively. AD, Activating domain; BD, binding domain. B, The BiLC shows that ZmNRPC2 and dNRPC2 interact with RPC53, AC40, TFC1, and FL3. Fluorescence signal intensities represent their interaction affinity. C, RT-qPCR analysis of 17 tRNA and 5S rRNA genes in 15-DAP endosperm of wild type and *smk7*. All expression levels are normalized to *ACTIN*. Three replicates for each sample were assessed and data are means ± SD. Asterisks indicate significant difference by Student's *t* test (*$P < 0.05$, **$P < 0.01$, and ***$P < 0.01$).

Transcriptomic Alterations in the *smk7* Endosperm

To reveal the function of *smk7*, we performed RNA sequencing (RNA-seq) using endosperm cells from *smk7*, *fl3*, *smk7;fl3*, and wild-type kernels at 15 DAPS on the same F1 ears. Differentially expressed genes (DEGs) were identified as those with a threshold fold change greater than two times at $P < 0.01$. Compared with wild type, 3,009 and 7,927 DEGs were identified in *smk7* and *fl3*, respectively. Notably, 1,478 (49.1%) DEGs were common to *smk7* and *fl3* (Fig. 8A), indicating that *smk7* and *fl3* share overlapping functions. Gene ontology (GO) analysis showed that these DEGs were mainly related to DNA-dependent replication (GO:0006261, false discovery rate [FDR]: 3.21E-06), DNA replication initiation (GO:0006270, FDR: 2.97E-03), and recombinational repair (GO:0000725, FDR: 1.89E-03; Fig. 8B). According to the Kyoto Encyclopedia of Genes and Genomes (KEGG; https://www.kegg.jp/) analysis, these DEGs were primarily related to DNA replication, fatty acid biosynthesis, and metabolism (Fig. 8C). Multiple key genes involved in DNA replication and the cell cycle were differentially expressed in the three mutants, such as those belonging to the minichromosome maintenance (MCM) 2-7 gene family, the proliferating cell nuclear antigen (PCNA) subunit of DNA polymerase δ, RBR protein, and cyclins. The MCM2-7 complexes bind to the origin region to form the DNA prereplication complex (Kusunoki and Ishimi, 2014). The expression of 10 *MCM2-7* genes increased by more than 2-fold in *smk7* and *smk7;fl3* and five *MCM2-7* genes were upregulated in *fl3* (Fig. 8D). The PCNA protein functions as the hub protein in the replication fork (Boehm et al., 2016), and *PCNA1* and *PCNA2* were upregulated all three mutants (Fig. 8D). However, RBR3, which plays a positive role in E2F-dependent gene expression and DNA replication, was upregulated in the three mutants (Fig. 8D; Sabelli et al., 2009). Previous study showed that RBR3, PCNA, and MCM2-7 positively regulate endoreduplication in maize and Arabidopsis (*Arabidopsis thaliana*; Park et al., 2005; Sabelli et al., 2013). In *smk7*, all flow cytometry peaks examined were substantially less pronounced than in wild type, suggesting that the mean ploidy of the endosperm nuclei was higher in mutant endosperm and that endoreduplication is affected by *zmnrpc2* (Supplemental Fig. S7). These results demonstrate that both *fl3* and *smk7* affect DNA replication.

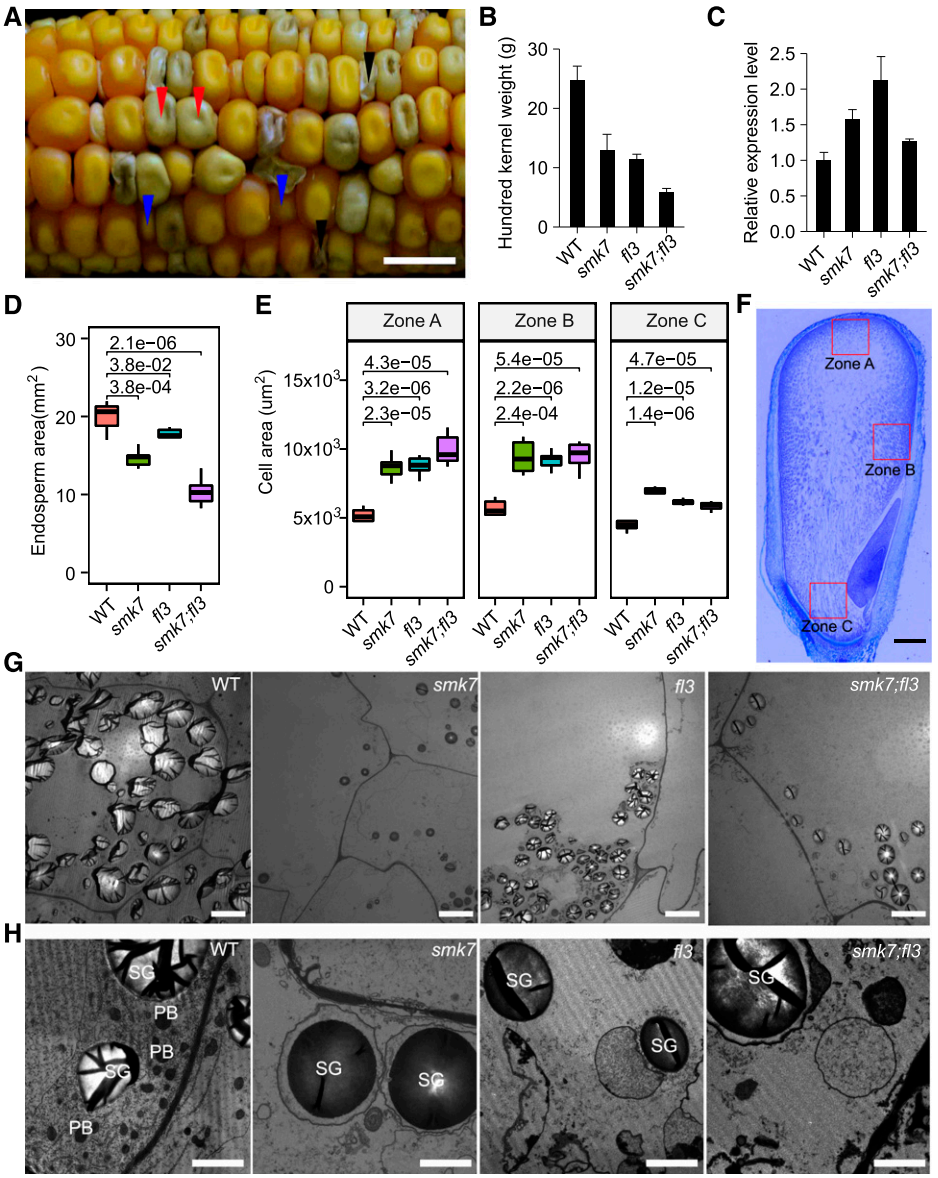

Figure 6. Phenotype of *smk7*;*fl3* kernels. A, Mature F2 ear of *smk7* × *fl3*. Red, blue, and black arrows indicate *fl3*, *smk7*, and *smk7*;*fl3* kernels, respectively. Scale bar = 1 cm. B, Comparison of the 100-kernel weight of randomly selected mature wild-type (WT), *fl3*, *smk7*, and *smk7*;*fl3* kernels in a segregating F2 population. Values are means ± SE. $n = 6$. *P* value determined by Student's *t* test. C, RT-qPCR analysis of *ZmNRPC2* genes in 15-DAP endosperm of wild type, *smk7*, *fl3*, and *smk7*;*fl3*. All expression levels are normalized to ACTIN. Three replicates for each sample were performed and data are means ± SD. *P* value determined by Student's *t* test. D, Endosperm area of wild type, *fl3*, *smk7*, and *smk7*;*fl3* at 15 DAP. *P* value determined by Student's *t* test. E, Cell area of wild type, *fl3*, *smk7*, and *smk7*;*fl3* at 15 DAPS. Zone A, Top of the kernel; Zone B, peripheral regions of the kernel; Zone C, base of the kernel. *P* value determined by Student's *t* test. F, Cell areas were measured in three endosperm zones (Zones A–C). Scale bar = 1,000 μm. G, Transmission electron microscopy of 15-DAP endosperm of wild type, *fl3*, *smk7*, and *smk7*;*fl3*. Scale bars = 10 μm. H, Transmission electron microscopy of the magnified startch granule (SG) and protein body (PB) in wild type, *fl3*, *smk7*, and *smk7*;*fl3*. Scale bars = 2 μm.

To investigate the different functions of *smk7* and *fl3* in maize endosperm development, GO and KEGG analyses were performed using the *smk7* DEGs (1,531) and *fl3* DEGs (6,449). GO categories that were related to cell proliferation, such as mitotic cell cycle process, mitotic nuclear division, cell population proliferation, and DNA replication, as well as MCM complex and DNA packaging complex, were highly enriched among *smk7* DEGs (Fig. 8B), and were shared by DEGs in double mutants. Furthermore, 12 cyclins were upregulated in *smk7* and *smk7*;*fl3* (Fig. 8D), confirming that *smk7* affects cell proliferation. However, *fl3* DEGs were mainly related to small molecule metabolic process, lipid biosynthetic process, organic acid metabolic process, oxoacid metabolic process, and peroxisome categories (Fig. 8B). Some key genes involved in protein biosynthesis were significantly downregulated in *fl3* and *smk7*;*fl3*, including *Opaque5* (*O5*), *O11*, *O7*, *Oxalyl-CoA Decarboxylase1* (*OCD1*), *Naked endosperm1* (*Nkd1*), *Pyruvate Orthophosphate Dikinase1*, and *Pyruvate Orthophosphate Dikinase2* (Fig. 8D) and strikingly, five *CYCLIN* genes were upregulated in *fl3* (Fig. 8D). These results indicated that FL3 plays a major role in zein synthesis to control seed quality and might also affect cell proliferation.

DISCUSSION

Mutation of *ZmNRPC2* Affects Maize Endosperm Development

We have described a recessive mutant that represses endosperm cell proliferation, causes defects in the endosperm peripheral regions and BETL cell wall ingrowths, and compacts the length of the CZ cells (Fig. 1,

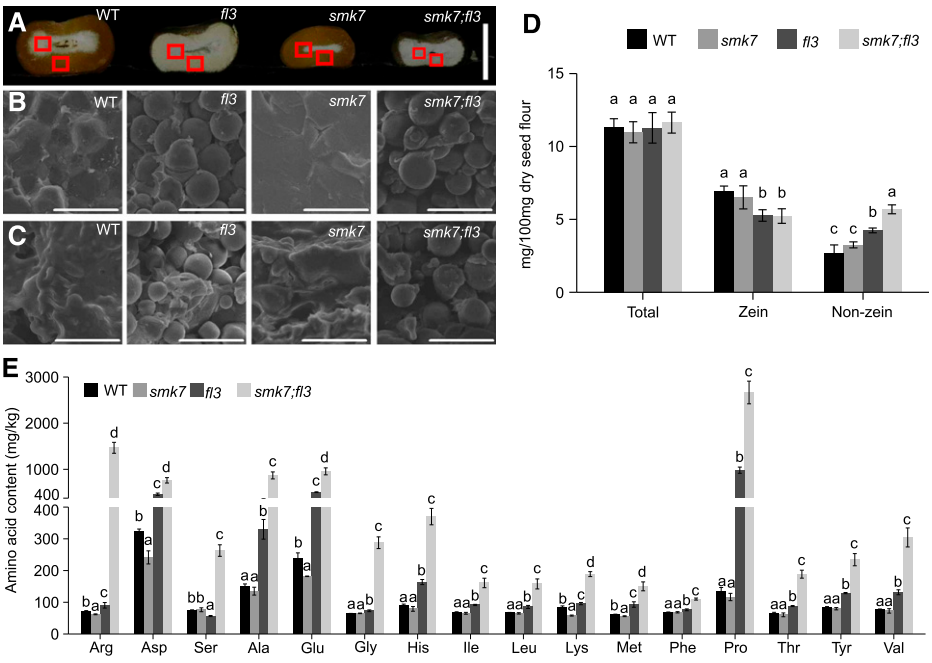

Figure 7. Comparison of zein and free amino acid content in wild-type (WT), *smk7*, *fl3*, and *smk7;fl3* kernels. A, Transverse sections of mature kernels of wild type, *fl3*, *smk7*, and *smk7;fl3* (from left to right). Scale bar = 3 mm. B and C, Scanning electron microscope images of the kernel peripheral regions (B) and central regions (C) indicated by the red-outlined boxes in A. Scale bars = 20 μm. D, Comparison of the protein content of mature wild-type, *fl3*, *smk7*, and *smk7;fl3* kernels. Values are means with ±SE. $n = 6$. Lowercase letters indicate significant difference as determined by Student's *t* test ($P < 0.01$). E, Comparison of free amino acid content of mature wild-type, *fl3*, *smk7*, and *smk7;fl3* kernels. Values are means with ±SE. $n = 3$. Lowercase letters indicate significant difference as determined by Student's *t* test ($P < 0.05$).

E–L). To date, most maize kernel mutants that have been characterized show either defects in storage reserve accumulation (e.g. the *opaque* and *floury* mutants), or incomplete seed development, which affects germination, such as *dek* or *empty pericarp* mutants (Zhang et al., 2016; Cai et al., 2017; Chen et al., 2017; Feng et al., 2018). Unlike those mutants, *smk7* affected neither kernel storage protein composition nor germination, but delayed endosperm development and in turn, led to lower kernel weight and smaller kernels. The BETL in the kernel is composed of two to three strata of highly elongated transfer cells with invaginated cell walls (McCurdy and Hueros, 2014), and transports nutrients from phloem termini in the pedicel to filial tissues (Felker and Shannon, 1980; Kang et al., 2009). In *smk7*, hardly any cell wall ingrowths of the BETL were observed, suggesting that nutrient transport from the vegetative tissues to kernels might be disrupted in *smk7* kernels, resulting in smaller storage protein bodies and starch granules. The wild-type CZ contains highly elongated cells (~3.5-times longer than they are wide), which are thought to transport nutrients throughout the endosperm (Becraft, 2001). Cells in the *smk7* CZ were shorter, especially in the region adjacent to the BETL. The AL cell layer forms at the surface of the endosperm and its main functions in cereals include storage, defense, and hydrolysis (Regvar et al., 2011; Brouns et al., 2012). AL defects block embryo and endosperm development (Becraft et al., 2002; Lid et al., 2002). The peripheral endosperm regions of the *smk7* contained some layers of small cells, which were stained lighter than cells in the AL, and were smaller than starch endosperm cells. These cells were thought to be defective endosperm cells, because the AL only consisted of a single cell layer at the region adjacent to embryo in *smk7* and wild type, and *smk7* lacks the feature of AL mutants. Notably, the features of the BETL, the CZ, and peripheral starch endosperm cells differed between *fl3* and *smk7*: Those in *fl3* were similar to those in wild type, and those in double mutants were more similar to those in *smk7* (Supplemental Fig. S6B). *ZmNRPC2* is widely spatiotemporally expressed in various tissues such as the placento-chalazal region, the AL, the CZ, and the central starchy endosperm; however, *FL3* is exclusively expressed in the central starchy endosperm (Supplemental Fig. S8; Zhan et al., 2015; Li et al., 2017c). Taken together, we suggest that *ZmNRPC2* controls endosperm development by regulating the BETL, CZ, and the growth and function of starchy endosperm cells, providing a novel entry point to understand seed development.

ZmNRPC2 Is Essential for RNAPIII Function

The two largest polypeptides in RNAPIII, NRPC1, and NRPC2 form the binding cleft for DNA and harbor the active site of the enzyme, which fosters catalytic phosphodiester bond formation during the transcription of genes encoding small noncoding RNA molecules (Vannini and Cramer, 2012). In mice, mutation of *NRPC2* reduced the cell proliferation in neonatal intestinal epithelium; in zebra fish, mutation of *NRPC2* caused cell cycle abnormal in highly proliferative tissues, such as the liver, retina, and terminal branchial arches; in Arabidopsis, mutation of *NRPC2* caused female gametophyte developmental arrest (Yee et al., 2007; Onodera et al., 2008; Kieckhaefer et al., 2016). In this study, *smk7*, *nrpc2-KO2*, and *nrpc2-KO3* defects of three different positions in the conserved RNA_pol_Rpb2_7 domain of ZmNRPC2 suppressed the cell proliferation in endosperm and caused the small kernel

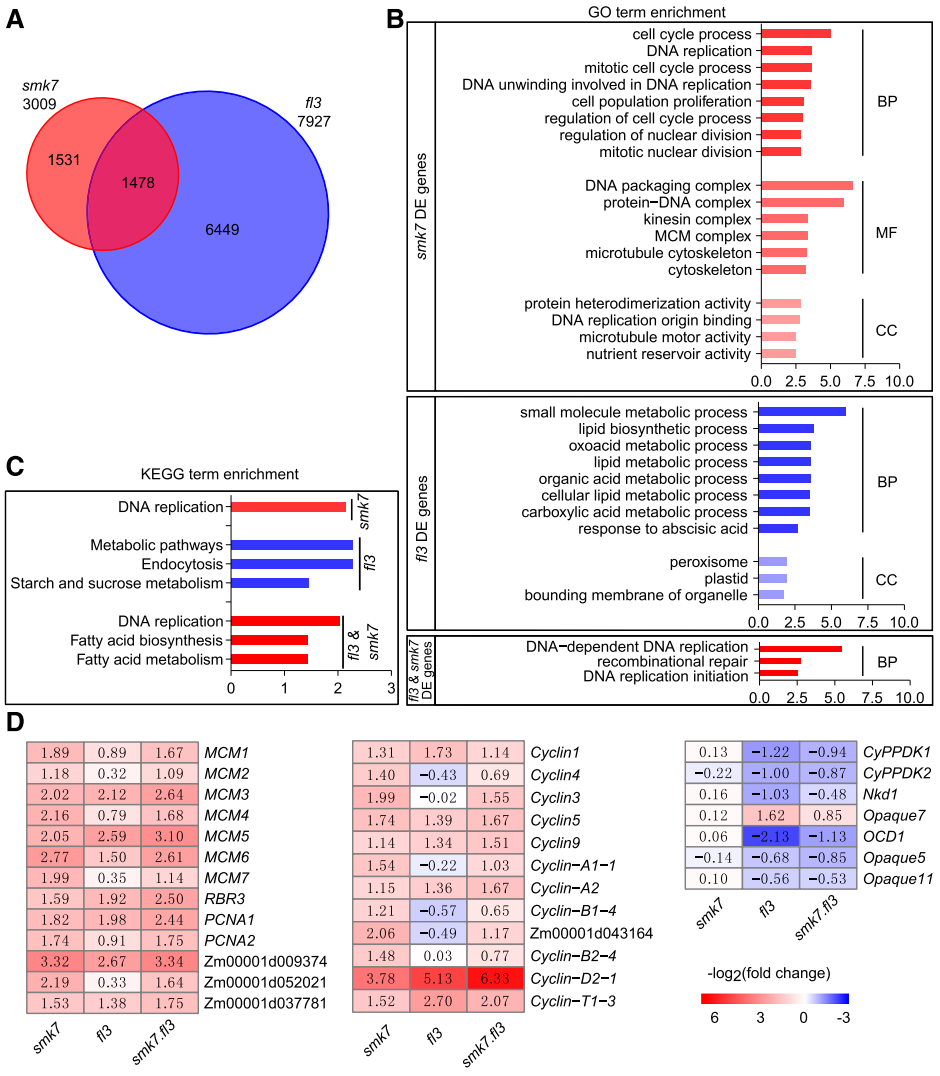

Figure 8. Global transcriptome analysis based on RNA-seq data and cell area in 15-DAP endosperm of wild-type, *fl3*, *smk7*, and *smk7*; *fl3* kernels in a segregating F2 population. A, The numbers of DEGs in *fl3* and *smk7* endosperm compared with the wild type. B, GO classification for genes with differentially expression in the *fl3*, *smk7*, and *fl3*;*smk7* endosperm compared with the wild type. *x* axis, $-\log_{10}$(FDR). C, Significantly enriched KEGG terms among genes whit differential expression in the *fl3*, *nrpc2*, and *fl3*;*smk7* endosperm compared with the wild type. *x* axis, $-\log_{10}$(FDR). D, Log_2-fold change heat maps of DEGs functioning in selected disrupted pathways in three types mutants. displayed numbers; $-\log_2$-fold change.

phenotype; in addition, in *nrpc2-KO1*, deletion of this protein can result in kernel developmental arrest. Meanwhile, *zmnrpc2* affects kernel development more seriously than seedling growth. All the above results indicate that normal ZmNRPC2 protein is essential during the kernel rapid development stage. Similar phenomena have been observed in Treacher–Collins syndrome, in which RNA polymerases mutation affects the proper formation of the first and second branchial arches at weeks 5 to 8 of fetal development (Kadakia et al., 2014).

RNAPIII comprises 17 subunits that include the conserved 10-subunit core, the stalk, and two additional subcomplexes. The composition of RNAPIII is conserved throughout eukaryotes (Ream et al., 2015). The NRPC2 protein is associated with the largest subunit of RNAPIII and provides a platform for the assembly of other subunits/subcomplexes (Hardeland and Hurt, 2006; Cieśla et al., 2015). The data here confirmed the functions of homologous NRPC2 in maize and showed that ZmNRPC2 interacts with three critical RNAPIII subunits, RPC53, AC40, and TFC1 (Fig. 5, A and B). The RPC53–RPC37 heterodimer is positioned within the lobe of RNAPIII, close to the active site, the stalk, and the heterotrimer, and plays an important role in RNAPIII transcription termination, reinitiation, and elongation, as well as promoter accessibility (Wu et al., 2011, 2012; Arimbasseri et al., 2014). The AC40 protein is a component of the 10-subunit enzymatic core (Vannini and Cramer, 2012). TFC1 is a subunit of TFIIIC, which binds to the internal promoter elements and intragenic regions of tRNAs and 5S rRNAs for recruitment of TFIIIB and RNAPIII, and is required for transcription of tRNAs and 5S rRNAs (Male et al., 2015). These RNAPIII subunits might be degraded when they are not assembled or are misassembled into the complex, as was observed for mutants defective in the assembly of the RNAPII complexes, in which the largest RNAPII subunit underwent nuclear degradation (Garrido-Godino et al., 2013). ZmNRPC2 also interacted with FL3, which functions as a regulator within the RNAPIII transcription machinery and controls tRNAs and 5S rRNA levels (Li et al., 2017c).

These results indicate that NRPC2 is the central core of RNAPIII in maize.

RNAPIII Affects Cell Proliferation and Endoreduplication in Maize Endosperm

The normal transcription of 5sRNA and tRNAs is critical to maintain efficient running of the protein synthesis system, which guarantees the need for protein during DNA replication. The process of cell proliferation and endoreduplication, which relies on DNA replication, ensure the normal development of endosperm (Lopes and Larkins, 1993; Park et al., 2005; Sabelli et al., 2009). Our data indicates that the decreased expression level of *ZmNRPC2* or loss of *FL3* function suppressed the transcription of 5sRNA and tRNAs (Supplemental Fig. S9), which affects protein synthesis thus influencing DNA replication, the mitotic cell cycle, and endoreduplication (Fig. 8B), eventually leading to defective endosperm development and small kernel size. This differs from several signaling pathways that determine seed size, such as the Leu-rich repeat kinase pathway, the ubiquitin–proteasome pathway, and G-protein signaling (Li and Li, 2016; Li et al., 2019), and represents a novel pathway in the control of seed size. Maize endosperm development undergoes two major mitotic cell cycles—the coenocytic and cellularization stages. Nuclei of the coenocytic endosperm divide rapidly but no cytokinesis occurs (until ~2–4 DAP), resulting in a single multinucleate cell. This phase is dependent on rapid DNA replication (Lopes and Larkins, 1993; Brown et al., 2003; Olsen, 2004). At cellularization, mitotic cell division causes the number of endosperm cells to increase dramatically, to generate the vast majority of starchy endosperm cells, but the total number of cells is also influenced by the coenocytic phase (Kowles and Phillips, 1985). Therefore, the number of endosperm cells might be influenced by the level of DNA replication. In *smk7* and *fl3*, there were considerably fewer endosperm cells, whereas the expression levels of many genes involved in DNA replication and the mitotic cell cycle increased. Furthermore, the relationship between the low transcriptional activity of RNAPIII and cell proliferation defects have been confirmed in mice and zebrafish (*Danio rerio*; Yee et al., 2007; Kieckhaefer et al., 2016).

Endoreduplication is a specialized type of cell cycle, in which one or more rounds of DNA synthesis are performed without mitosis, resulting in polyploid cells (Larkins et al., 2001). A strong correlation between endoreduplication and cell size has been observed in the maize endosperm (Sabelli et al., 2013; He et al., 2019). In *smk7*, endoreduplication was affected and the endosperm cells were larger; furthermore, expression of *MCM2-7*, *RBR3*, *PCNA1*, and *PCNA2* increased considerably in mutant kernels. In maize and Arabidopsis, RBR3, PCNA, and MCM2-7 positively regulate endoreduplication (Park et al., 2005; Sabelli et al., 2013); and RBR1 negatively regulates these DNA replication factors to stimulate nuclear and cell enlargement and control endosperm development in maize (Sabelli et al., 2013). These findings indicated that RNAPIII affects cell cycle and endosperm development in maize (Fig. 9).

RNAPIII Affects Storage Reserve Filling in Maize Kernel

Intriguingly, several well-characterized opaque endosperm genes such as *O7*, *O11*, *OCD1*, and *NKD1*

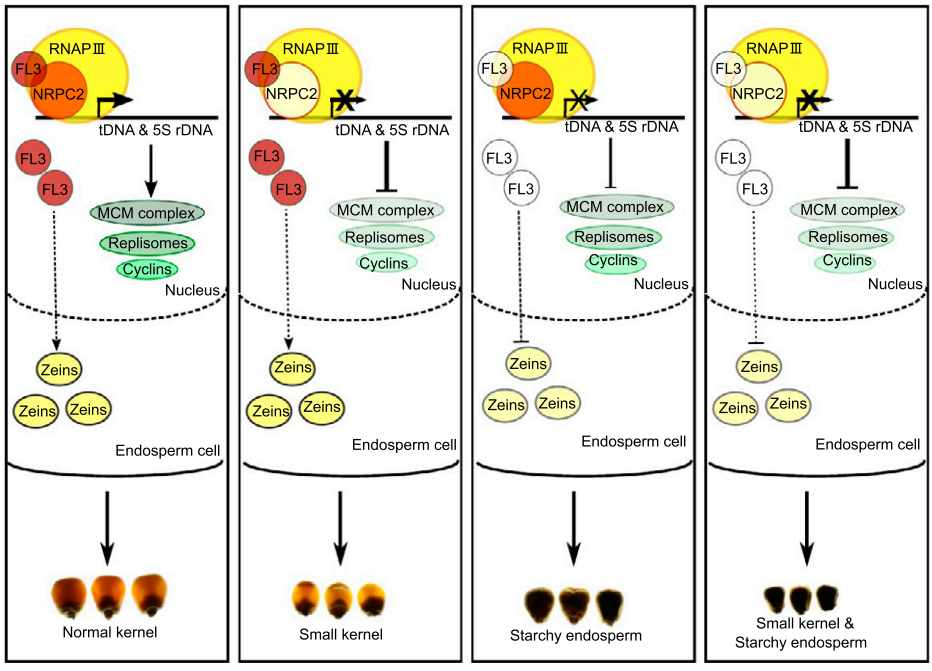

Figure 9. Proposed model for how ZmNRPC2 and FL3 control endosperm development and grain filling in the maize kernel. RNAPIII affects cell cycle and endosperm development in maize. NRPC2 and FL3 is key factor of the RNAPIII transcription machinery. The biogenesis of tRNAs and 5S rRNA was significantly reduced by the *nrpc2* and *fl3* mutation, then affect cell cycle and endosperm development.

were significantly downregulated in *fl3* and *smk7;fl3* endosperm. The *o5*, *o11*, *ocd1*, and *nkd1* mutants have kernels with an opaque endosperm, which is consistent with the *fl3* and *smk7;fl3* phenotype (Myers et al., 2011; Yi et al., 2015; Feng et al., 2018; Yang et al., 2018). *O7* expression was significantly upregulated in the *fl3* and *smk7;fl3* endosperm, and *o7* also has an opaque endosperm (Wang et al., 2011). Notably, *OCD1* acts downstream of O7 and encodes oxalyl-CoA decarboxylase, which catalyzes the breakdown of oxalyl-CoA into formyl-CoA and CO_2 (Yang et al., 2018). We observed that genes involved in oxoacid metabolism were significantly enriched in *fl3* DEGs (Fig. 8). Similarly, *fl3* and *smk7;fl3* possess an opaque endosperm with a reduced zein protein content, but *smk7* has a normal endosperm. This might be caused by defects in different subunits of RNAPIII (Fig. 9) and suggests that RNAPIII potentially plays a role in affecting maize kernel development and storage reserve filling.

MATERIALS AND METHODS

Plant Material

All maize (*Zea mays*) plants were grown either in plastic greenhouses in Wuhan, China or in the field in Huanggang and Sanya, China. The temperature in the greenhouse was 25°C to 32°C during maize pollination and the early developmental stage. The pollen of the Mo17 inbred line was collected and mutagenized with ethyl methanesulfonate for 30 min and was then applied to Mo17 female ears. All seeds were planted and self-pollinated and a single ear segregated mutant seeds with small kernels and the mutant was designated *smk7*. To eliminate unassociated mutations, *smk7* was recurrently backcrossed to Mo17 (used as the female) for four generations. The *smk7* mutant was crossed into the B73 inbred line and kernels were collected from a self-pollinated *smk7*/+ ear in the B73 genetic background.

Genetic Mapping of the *smk7* Locus

Initial mapping of *smk7* was performed using bulk-sequence analysis with the pooled DNA samples extracted from the endosperm of 30 mutant kernels and 30 wild-type kernels from a segregating F2 ear. Genomic DNA was sheared for preparation of the sequencing library according to the standard protocol of the Illumina TruSeq DNA PCR-free prep kit. Reads of the two bulks were aligned to the reference genome (maize B73 RefGen_v4) using the software bwa (v.0.7.15; https://github.com/lh3/bwa) with default parameters; SNP calling was performed using the software GATK (v.3.3.0; http://www.broadinstitute.org/gatk). SNPs with a sequencing depth of <5 were filtered. Then, the SNP index was calculated, and SNPs with an SNP index of <0.3 in both bulks were filtered to reduce false-positive detection of SNPs. The delta-SNP index was determined by the difference between the mutant and wild-type bulk. The mean delta-SNP index was calculated using a sliding-window approach with a 500-SNP window size and a 50-SNP increment. The *zmnrpc2* mutation was mapped to a 63.64-Mb interval on chromosome 6 (from 19,352,816 to 83,002,397; maize B73 RefGen_v4). Markers were developed within this interval, and 300 kernels were used to narrow the candidate interval to 25 Mb. Additional markers were developed within this interval, and a total of 4,000 mutant kernels from the F2 population were used to narrow down the *ZmNRPC2* locus to a 2.61-Mb interval (from 61,269,234 to 63,875,645).

RNA Extraction and RT-qPCR

Immature embryo and endosperm from three independent kernels were quickly frozen in liquid nitrogen and were ground into a fine powder with a mortar and pestle. The wild-type and *zmnrpc2* immature kernels were identified by genotyping using SNP62,672,025. Total RNA was extracted with 1 mL of TRIzol reagent (Thermo Fisher Scientific) according to the manufacturer's instructions. After isopropanol precipitation, the RNA was resuspended in 50 μL of RNase-free water and treated with RNase-free DNase I. For reverse transcription, 1 μg of total RNA was used in each 20-μL reaction and the first cDNA strand was synthesized using SuperScriptII (Invitrogen) and hexamer primers according to the manufacturer's instructions. SYBR Green (Bio-Rad) was added to PCR reaction according to the guidelines. The RT-qPCR analysis was carried out with three independent RNA samples using a Bio-Rad CFX96 Touch Real-Time PCR detection system using *ZmActin1* as an internal control, and the relative expression of mRNA was calculated using the $2^{-\Delta\Delta Ct}$ method (Livak and Schmittgen, 2001). Expression of 5S rRNA and tRNAs was analyzed via RT-qPCR using previously described primers (Li et al., 2017c). The primers used for RT-qPCR of *ZmNRPC2* expression are listed in Supplemental File S2.

Subcellular Localization of ZmNRPC2

To generate a translational ZmNRPC2-GFP and dNRPC2-GFP fusion, we amplified the full-length ORFs of *ZmNRPC2* and *dNRPC2* lacking the stop codons by PCR using cDNA from the inbred line Mo17 and *smk7*, respectively, and cloned them into pM999-GFP under control of the cauliflower mosaic virus 35S promoter. Maize mesophyll protoplasts were isolated from etiolated leaves by digestion with an enzyme solution (1.5% [w/v] cellulose R10, 0.3% [w/v] pectolyase Y23, 20 mM of MES at pH 5.7, 0.4 M mannitol, 20 mM KCl, 10 mM $CaCl_2$, and 0.1% [w/v] BSA). The plasmids containing the ZmNRPC2-GFP and dNRPC2-GFP fusion constructs were transfected into the protoplasts using established protocols (Yoo et al., 2007). The transfected protoplasts were cultured at 25°C overnight and GFP and Tracker red signals were detected with a FluoView FV1200 confocal microscope (Olympus).

Cytological Observation

Kernels at 8, 10, 12, 15, 18, and 21 DAP were collected and cut along the longitudinal axis. The cut kernels were fixed overnight in 4% (v/v) paraformaldehyde (Sigma-Aldrich), dehydrated in an ethanol gradient series (30%, 50%, 70%, 85%, 95%, and 100% [v/v] ethanol), and embedded in Paraplast Plus (Sigma-Aldrich). The sample blocks were sectioned into 8-μm slices using a model no. RM2265 microtome (Leica Microsystems) and stained with 0.5% (w/v) toluidine blue O. Images were captured using a model no. MZFLIII microscope (Leica Microsystems). Additionally, for transmission electron microscopy analysis, endosperms at 15 DAP were cut into 1-mm^3 pieces. Fresh tissues were fixed overnight in 2.5% (w/v) glutaraldehyde in 0.1 M of phosphate buffer at pH 7.4, fixed in 2% (w/v) OsO_4 in the same buffer, and then dehydrated and embedded in epoxy resin and SPI-812 (Structure Probe). Ultrathin sections obtained using a model no. UC6 ultra microtome (Leica Microsystems) were stained with uranyl acetate and subsequently with lead citrate. The observations and recording of images were performed using a model no. H-7650 transmission electron microscope (Hitachi) at 80 kV and a 832-CCD camera (Gatan). The procedures were performed as described by Yi et al. (2010). For scanning electron microscopy analysis, mature wild-type and mutant kernels were excised with a razor, sputter-coated with gold in an E-100 ion sputtering process, and observed with a scanning electron microscope (S3400N; Hitachi).

Vector Construction for Maize Transformation

We performed CRISPR/Cas9–based gene editing of *Zm00001d035960*, with three guide RNAs to target the insertion, using pCPB-ZmUbi-hspCas9 (Li et al., 2017a). For CRISPR/Cas9–edited plants, sequencing was used to identify the editing sites near the target position.

Measurement of Proteins, Soluble Sugars, Starch, and Soluble Amino Acids

Mature mutant and wild-type kernels were collected from the same segregating ears. A total of 30 mutant and wild-type endosperms from the same ear were pooled as a single replicate, the seed coats and embryos were removed from the kernels after soaking in water for 10 min and were ground into a fine powder in liquid nitrogen. Six biological replicates were used for subsequent analysis. A 50-mg sample was incubated overnight in 1 mL of lysis buffer (12.5 mM of sodium borate, 1% [w/v] SDS, 2% [v/v] β-mercaptoethanol, 1% [w/v] cocktail [Merck], and 1% [w/v] phenylmethylsulfonyl fluoride) in a 37°C shaker. The mixture was centrifuged for 15 min at 13,000*g* after which 300 μL of supernatant was carefully transferred into two different 1.5-mL centrifuge

tubes. One tube was used to estimate total protein; 700 μL of ethanol was added to the other tube, which was then incubated at 25°C on a shaker for 3 h and was centrifuged for 15 min at 13,000*g*. The supernatant contained zeins and the precipitate, nonzeins. The amount of zein and nonzein proteins were quantified using the Modified BCA Protein Assay Kit (Sangon Biotech). Starch quantification was performed using the amyloglucosidase/α-amylase starch assay kit (Megazyme). Soluble amino acids were analyzed according to the method of Palmero et al. (1992).

Flow Cytometry

The endosperm was finely chopped using a razor blade in 1 mL of ice-cold Galbraith's buffer (45 mM of $MgCl_2$, 20 mM of MOPS, 30 mM of sodium citrate, and 0.1% [v/v] Triton X-100, adjusted to pH 7.0 using 1 M of NaOH, and filtered through a 0.22-mm filter) in a glass petri dish. The homogenate was filtered through a 42-mm nylon mesh into a 1.5-mL sample tube. Propidium iodide and RNase were added to a final concentration of 50 mg mL^{-1}, after which the tubes were shaken gently. The homogenate was measured immediately using a flow cytometer (MoFlo XDP; Beckman Coulter), with an argon-ion laser tuned to 488 nm. A total of 15,000 particles were collected and analyzed using the software Summit v.5.2 (http://www.cyto.purdue.edu/cdroms/cyto5/sponsors/cytomate/summit.htm).

Y2H Assay and BiLC

For Y2H assays, the *ZmNRPC2* coding sequence was cloned into the pGBKT7 plasmid and transformed into the yeast strain Y2HGold, whereas the coding sequence encoding the other RNAP subunit and FL3 were inserted into the pGADT7 plasmid and transformed into the yeast strain Y187. All yeast experiments were referenced in Clontech's Yeast Protocols Handbook.

To create constructs for BiLC experiments, the *ZmNRPC2* coding sequence was cloned into JW772 (C-terminal half of luciferase [CLUC]) to yield *ZmNRPC2-CLUC* and sequences encoding the other RNAPIII subunit and FL3 were cloned into JW771 (N-terminal half of luciferase). The appropriate pairs of CLUC or N-terminal half of luciferase fusion constructs were used for the luciferase complementation assay, following the protocol described in Gou et al. (2011). *Agrobacterium tumefaciens* (strain GV3101) harboring the above constructs was infiltrated into leaves from 3-week–old *Nicotiana benthamiana* plants using a needleless syringe. After incubating for 72 h under 16-h light:8-h dark, leaves were injected with 0.8 mM of luciferin and the resulting luciferase signals were captured using a Tanon-5200 system (Tanon Science and Technology). These experiments were repeated at least three times with similar results. Quantitative analysis was performed using the software ImageJ (http://rsb.info.nih.gov/ij/).

RNA-Seq Analysis

Total RNA was extracted from pooled wild-type and mutant endosperm obtained from the same F2 ears derived from the cross *nrpc2* × *fl3* at 15 DAP (10 kernels per sample) using TRIzol reagent, followed by cleanup and DNase I treatment using an RNeasy Mini Kit (Qiagen), according to the manufacturer's protocol. The different types of immature kernels were identified by genotyping using SNP62,672,025 and SNP6585. Three independent biological replicates from three different ears were performed. cDNA libraries were constructed following the standard Illumina protocol and sequenced on the Illumina NovaSeq platform by Novogene. The sequence reads were trimmed using the tool Trimmomatic (v.0.33; http://www.usadellab.org/cms/?page=trimmomatic) and were mapped to the B73 RefGen_v4.34 reference genome using the program HISAT2 (v.2.1.0; http://ccb.jhu.edu/software/hisat2/faq.shtml). The program StringTie (v.1.3.3b) was employed to reconstruct the transcripts and to estimate gene expression levels (Pertea et al., 2016). The program HTSeq (v.0.6.1; https://pypi.org/project/HTSeq/) was used to count the number of reads per gene. Significant DEGs were identified by DEseq2 (http://www.bioconductor.org/packages/devel/bioc/html/DESeq2.html) as those with a *P* value of differential expression above the threshold ($P < 0.01$, absolute value of $\log_2$[fold change] > 1). The conjoint GO and KEGG term enrichment results were generated using the software "g:Profiler" (http://biit.cs.ut.ee/gprofiler/).

Accession Numbers

Sequence data from this article can be found in the GenBank/EMBL data libraries under accession numbers XP_008648749 for NRPC2, NM_001152112 for FL3, XM_008669830 for RPC53, XM_008663148 for TFC1, and NP 001130839 for AC40. Sequences used for phylogenetic analysis are as follows: XP_003570586.1, *Brachypodium distachyon*; XP_015632810.1, *Oryza sativa Japonica Group*; XP_004951189.1, *Setaria italica*; XP_021305150.1, *Sorghum bicolor*; XP_008648749.1, *Z. mays*; XP_024627527.1, *Medicago truncatula*; XP_006583557.1, *Glycine max*; XP_017615303.1, *Gossypium arboreum*; XP_010659064.1, *Vitis vinifera*; NP_001332060.1, *Arabidopsis thaliana*; XP_020077589.1, *Hyphopichia burtonii*; NP_014850.1, *Saccharomyces cerevisiae*; XP_021323450.1, *Danio rerio*; XP_014263402.1, *Maylandia zebra*; NP_001154180.1, *Homo sapiens*; XP_004006743.1, *Ovis aries*; NP_081699.1, *Mus musculus*; XP_002904335.1, *Phytophthora infestans*, and PRJNA639712 for RNA-seq data.

Supplemental Data

The following supplemental materials are available.

Supplemental Figure S1. Phenotype of *smk7* kernels and plants.

Supplemental Figure S2. Kernel phenotypic inheritance and a comparison of developing wild-type and smk7 kernels at different development stages.

Supplemental Figure S3. Protein structure and three-dimensional structure of NRPC2.

Supplemental Figure S4. Allelism test between *smk7* and *ZmNRPC2* knockout alleles.

Supplemental Figure S5. Subcellular localization of NRPC2/*nrpc2* in maize leaf cells.

Supplemental Figure S6. Kernel phenotype of *smk7*;*fl3*.

Supplemental Figure S7. Flow cytometry profiles of wild-type and smk7 endosperm at 10 and 12 DAP.

Supplemental Figure S8. Spatial expression pattern of ZmNRPC2 and FL3 in maize kernels.

Supplemental Figure S9. Expression level of 17 tRNAs and 5S rRNA genes in 15-DAP endosperm of the wild type, *fl3*, *smk7*, and *smk7*;*fl3*.

Supplemental File S1. The full alignment file for estimating the NRPC2 protein sequences phylogenies used in this study.

Supplemental File S2. Primers used in this study.

ACKNOWLEDGMENTS

We thank Suhua Yang (Plant Science Facility of the Institute of Botany, Chinese Academy of Sciences) for her excellent technical assistance of flow cytometry. We also thank Plant Editors (https://planteditors.com/) for manuscript editing.

Received April 27, 2020; accepted June 15, 2020; published June 26, 2020.

LITERATURE CITED

Abascal-Palacios G, Ramsay EP, Beuron F, Morris E, Vannini A (2018) Structural basis of RNA polymerase III transcription initiation. Nature **553:** 301–306

Arimbasseri AG, Rijal K, Maraia RJ (2014) Comparative overview of RNA polymerase II and III transcription cycles, with focus on RNA polymerase III termination and reinitiation. Transcription **5:** e27639

Bai F, Corll J, Shodja DN, Davenport R, Feng G, Mudunkothge J, Brigolin CJ, Martin F, Spielbauer G, Tseung CW, et al (2019) RNA binding motif protein 48 is required for U12 splicing and maize endosperm differentiation. Plant Cell **31:** 715–733

Becraft PW (2001) Cell fate specification in the cereal endosperm. Semin Cell Dev Biol **12:** 387–394

Becraft PW, Li K, Dey N, Asuncion-Crabb Y (2002) The maize dek1 gene functions in embryonic pattern formation and cell fate specification. Development **129:** 5217–5225

Boehm EM, Gildenberg MS, Washington MT (2016) The many roles of PCNA in eukaryotic DNA replication. Enzymes **39:** 231–254

Brouns F, Hemery Y, Price R, Anson NM (2012) Wheat aleurone: Separation, composition, health aspects, and potential food use. Crit Rev Food Sci Nutr **52:** 553–568

Brown RC, Lemmon BE, Nguyen H (2003) Events during the first four rounds of mitosis establish three developmental domains in the syncytial endosperm of *Arabidopsis thaliana*. Protoplasma **222:** 167–174

Cai M, Li S, Sun F, Sun Q, Zhao H, Ren X, Zhao Y, Tan BC, Zhang Z, Qiu F (2017) Emp10 encodes a mitochondrial PPR protein that affects the cis-splicing of nad2 intron 1 and seed development in maize. Plant J **91:** 132–144

Chen X, Feng F, Qi W, Xu L, Yao D, Wang Q, Song R (2017) Dek35 encodes a PPR protein that affects cis-splicing of mitochondrial nad4 intron 1 and seed development in maize. Mol Plant **10:** 427–441

Cieśla M, Makała E, Płonka M, Bazan R, Gewartowski K, Dziembowski A, Boguta M (2015) Rbs1, a new protein implicated in RNA polymerase III biogenesis in yeast *Saccharomyces cerevisiae*. Mol Cell Biol **35:** 1169–1181

Ciganda M, Williams N (2011) Eukaryotic 5S rRNA biogenesis. Wiley Interdiscip Rev RNA **2:** 523–533

Cramer P, Bushnell DA, Kornberg RD (2001) Structural basis of transcription: RNA polymerase II at 2.8 angstrom resolution. Science **292:** 1863–1876

Dieci G, Fiorino G, Castelnuovo M, Teichmann M, Pagano A (2007) The expanding RNA polymerase III transcriptome. Trends Genet **23:** 614–622

Dieci G, Giuliodori S, Catellani M, Percudani R, Ottonello S (2002) Intragenic promoter adaptation and facilitated RNA polymerase III recycling in the transcription of SCR1, the 7SL RNA gene of *Saccharomyces cerevisiae*. J Biol Chem **277:** 6903–6914

Felker FC, Shannon JC (1980) Movement of C-labeled assimilates into kernels of *Zea mays* L: III. An anatomical examination and microautoradiographic study of assimilate transfer. Plant Physiol **65:** 864–870

Feng F, Qi W, Lv Y, Yan S, Xu L, Yang W, Yuan Y, Chen Y, Zhao H, Song R (2018) OPAQUE11 is a central hub of the regulatory network for maize endosperm development and nutrient metabolism. Plant Cell **30:** 375–396

Filer D, Thompson MA, Takhaveev V, Dobson AJ, Kotronaki I, Green JWM, Heinemann M, Tullet JMA, Alic N (2017) RNA polymerase III limits longevity downstream of TORC1. Nature **552:** 263–267

Garrido-Godino AI, García-López MC, Navarro F (2013) Correct assembly of RNA polymerase II depends on the foot domain and is required for multiple steps of transcription in *Saccharomyces cerevisiae*. Mol Cell Biol **33:** 3611–3626

Geiduschek EP, Kassavetis GA (2001) The RNA polymerase III transcription apparatus. J Mol Biol **310:** 1–26

Goodfellow SJ, White RJ (2007) Regulation of RNA polymerase III transcription during mammalian cell growth. Cell Cycle **6:** 2323–2326

Gou JY, Felippes FF, Liu CJ, Weigel D, Wang JW (2011) Negative regulation of anthocyanin biosynthesis in Arabidopsis by a miR156-targeted SPL transcription factor. Plant Cell **23:** 1512–1522

Hardeland U, Hurt E (2006) Coordinated nuclear import of RNA polymerase III subunits. Traffic **7:** 465–473

He Y, Wang J, Qi W, Song R (2019) Maize *Dek15* encodes the cohesin-loading complex subunit SCC4 and is essential for chromosome segregation and kernel development. Plant Cell **31:** 465–485

Hoffmann NA, Jakobi AJ, Moreno-Morcillo M, Glatt S, Kosinski J, Hagen WJ, Sachse C, Müller CW (2015) Molecular structures of unbound and transcribing RNA polymerase III. Nature **528:** 231–236

Huang Y, Wang H, Huang X, Wang Q, Wang J, An D, Li J, Wang W, Wu Y (2019) Maize VKS1 regulates mitosis and cytokinesis during early endosperm development. Plant Cell **31:** 1238–1256

Jiao Y, Peluso P, Shi J, Liang T, Stitzer MC, Wang B, Campbell MS, Stein JC, Wei X, Chin CS, et al (2017) Improved maize reference genome with single-molecule technologies. Nature **546:** 524–527

Kadakia S, Helman SN, Badhey AK, Saman M, Ducic Y (2014) Treacher-Collins syndrome: The genetics of a craniofacial disease. Int J Pediatr Otorhinolaryngol **78:** 893–898

Kang BH, Xiong Y, Williams DS, Pozueta-Romero D, Chourey PS (2009) Miniature1-encoded cell wall invertase is essential for assembly and function of wall-in-growth in the maize endosperm transfer cell. Plant Physiol **151:** 1366–1376

Karijolich J, Zhao Y, Alla R, Glaunsinger B (2017) Genome-wide mapping of infection-induced SINE RNAs reveals a role in selective mRNA export. Nucleic Acids Res **45:** 6194–6208

Kieckhaefer J, Lukovac S, Ye DZ, Lee D, Beetler DJ, Pack M, Kaestner KH (2016) The RNA polymerase III subunit Polr3b is required for the maintenance of small intestinal crypts in mice. Cell Mol Gastroenterol Hepatol **2:** 783–795

Kowles RV, Phillips RL (1985) DNA amplification patterns in maize endosperm nuclei during kernel development. Proc Natl Acad Sci USA **82:** 7010–7014

Kusunoki S, Ishimi Y (2014) Interaction of human minichromosome maintenance protein-binding protein with minichromosome maintenance 2-7. FEBS J **281:** 1057–1067

Larkins BA, Dilkes BP, Dante RA, Coelho CM, Woo YM, Liu Y (2001) Investigating the hows and whys of DNA endoreduplication. J Exp Bot **52:** 183–192

Li C, Liu C, Qi X, Wu Y, Fei X, Mao L, Cheng B, Li X, Xie C (2017a) RNA-guided Cas9 as an in vivo desired-target mutator in maize. Plant Biotechnol J **15:** 1566–1576

Li J, Fu J, Chen Y, Fan K, He C, Zhang Z, Li L, Liu Y, Zheng J, Ren D, et al (2017b) The U6 biogenesis-like 1 plays an important role in maize kernel and seedling development by affecting the 3′ end processing of U6 snRNA. Mol Plant **10:** 470–482

Li N, Li Y (2016) Signaling pathways of seed size control in plants. Curr Opin Plant Biol **33:** 23–32

Li N, Xu R, Li Y (2019) Molecular networks of seed size control in plants. Annu Rev Plant Biol **70:** 435–463

Li Q, Wang J, Ye J, Zheng X, Xiang X, Li C, Fu M, Wang Q, Zhang Z, Wu Y (2017c) The maize imprinted gene *Floury3* encodes a PLATZ protein required for tRNA and 5S rRNA transcription through interaction with RNA polymerase III. Plant Cell **29:** 2661–2675

Lid SE, Gruis D, Jung R, Lorentzen JA, Ananiev E, Chamberlin M, Niu X, Meeley R, Nichols S, Olsen OA (2002) The defective kernel 1 (dek1) gene required for aleurone cell development in the endosperm of maize grains encodes a membrane protein of the calpain gene superfamily. Proc Natl Acad Sci USA **99:** 5460–5465

Livak KJ, Schmittgen TD (2001) Analysis of relative gene expression data using real-time quantitative PCR and the $2^{-\Delta\Delta C(T)}$ method. Methods **25:** 402–408

Lopes MA, Larkins BA (1993) Endosperm origin, development, and function. Plant Cell **5:** 1383–1399

Male G, von Appen A, Glatt S, Taylor NM, Cristovao M, Groetsch H, Beck M, Müller CW (2015) Architecture of TFIIIC and its role in RNA polymerase III pre-initiation complex assembly. Nat Commun **6:** 7387

Mann C, Micouin JY, Chiannilkulchai N, Treich I, Buhler JM, Sentenac A (1992) RPC53 encodes a subunit of *Saccharomyces cerevisiae* RNA polymerase C (III) whose inactivation leads to a predominantly G1 arrest. Mol Cell Biol **12:** 4314–4326

Marshall L, White RJ (2008) Non-coding RNA production by RNA polymerase III is implicated in cancer. Nat Rev Cancer **8:** 911–914

McCurdy DW, Hueros G (2014) Transfer cells. Front Plant Sci **5:** 672

Myers AM, James MG, Lin Q, Yi G, Stinard PS, Hennen-Bierwagen TA, Becraft PW (2011) Maize opaque5 encodes monogalactosyldiacylglycerol synthase and specifically affects galactolipids necessary for amyloplast and chloroplast function. Plant Cell **23:** 2331–2347

Olsen O. A. (2004) Nuclear endosperm development in cereals and *Arabidopsis thaliana*. Plant Cell **16:** S214–S227

Onodera Y, Nakagawa K, Haag JR, Pikaard D, Mikami T, Ream T, Ito Y, Pikaard CS (2008) Sex-biased lethality or transmission of defective transcription machinery in Arabidopsis. Genetics **180:** 207–218

Palmero S, de Marchis M, Prati M, Fugassa E (1992) HPLC analysis of free amino acids and amino acids of total proteins in cultured cells: An application to the study of rat Sertoli cell protein metabolism. Anal Biochem **202:** 152–158

Park JA, Ahn JW, Kim YK, Kim SJ, Kim JK, Kim WT, Pai HS (2005) Retinoblastoma protein regulates cell proliferation, differentiation, and endoreduplication in plants. Plant J **42:** 153–163

Paule MR, White RJ (2000) Survey and summary: Transcription by RNA polymerases I and III. Nucleic Acids Res **28:** 1283–1298

Pavon-Eternod M, Gomes S, Geslain R, Dai Q, Rosner MR, Pan T (2009) tRNA over-expression in breast cancer and functional consequences. Nucleic Acids Res **37:** 7268–7280

Pertea M, Kim D, Pertea GM, Leek JT, Salzberg SL (2016) Transcript-level expression analysis of RNA-seq experiments with HISAT, StringTie and Ballgown. Nat Protoc **11:** 1650–1667

Ponicsan SL, Kugel JF, Goodrich JA (2010) Genomic gems: SINE RNAs regulate mRNA production. Curr Opin Genet Dev **20:** 149–155

Qi W, Lu L, Huang S, Song R (2019) Maize *Dek44* encodes mitochondrial ribosomal protein L9 and is required for seed development. Plant Physiol **180:** 2106–2119

Qi W, Yang Y, Feng X, Zhang M, Song R (2017) Mitochondrial function and maize kernel development requires Dek2, a pentatricopeptide repeat protein involved in nad1 mRNA splicing. Genetics **205:** 239–249

Ream TS, Haag JR, Pontvianne F, Nicora CD, Norbeck AD, Paša-Tolić L, Pikaard CS (2015) Subunit compositions of Arabidopsis RNA polymerases I and III reveal Pol I- and Pol III-specific forms of the AC40 subunit and alternative forms of the C53 subunit. Nucleic Acids Res **43:** 4163–4178

Regvar M, Eichert D, Kaulich B, Gianoncelli A, Pongrac P, Vogel-Mikus K, Kreft I (2011) New insights into globoids of protein storage vacuoles in wheat aleurone using synchrotron soft x-ray microscopy. J Exp Bot **62:** 3929–3939

Ren X, Pan Z, Zhao H, Zhao J, Cai M, Li J, Zhang Z, Qiu F (2017) EMPTY PERICARP11 serves as a factor for splicing of mitochondrial nad1 intron and is required to ensure proper seed development in maize. J Exp Bot **68:** 4571–4581

Sabelli PA, Hoerster G, Lizarraga LE, Brown SW, Gordon-Kamm WJ, Larkins BA (2009) Positive regulation of minichromosome maintenance gene expression, DNA replication, and cell transformation by a plant retinoblastoma gene. Proc Natl Acad Sci USA **106:** 4042–4047

Sabelli PA, Liu Y, Dante RA, Lizarraga LE, Nguyen HN, Brown SW, Klingler JP, Yu J, LaBrant E, Layton TM, et al (2013) Control of cell proliferation, endoreduplication, cell size, and cell death by the retinoblastoma-related pathway in maize endosperm. Proc Natl Acad Sci USA **110:** E1827–E1836

Vannini A, Cramer P (2012) Conservation between the RNA polymerase I, II, and III transcription initiation machineries. Mol Cell **45:** 439–446

Wang A, Hou Q, Si L, Huang X, Luo J, Lu D, Zhu J, Shangguan Y, Miao J, Xie Y, et al (2019) The PLATZ transcription factor GL6 affects grain length and number in rice. Plant Physiol **180:** 2077–2090

Wang G, Sun X, Wang G, Wang F, Gao Q, Sun X, Tang Y, Chang C, Lai J, Zhu L, et al (2011) Opaque7 encodes an acyl-activating enzyme-like protein that affects storage protein synthesis in maize endosperm. Genetics **189:** 1281–1295

Wang H, Wang K, Du Q, Wang Y, Fu Z, Guo Z, Kang D, Li WX, Tang J (2018) Maize Urb2 protein is required for kernel development and vegetative growth by affecting pre-ribosomal RNA processing. New Phytol **218:** 1233–1246

Wu CC, Herzog F, Jennebach S, Lin YC, Pai CY, Aebersold R, Cramer P, Chen HT (2012) RNA polymerase III subunit architecture and implications for open promoter complex formation. Proc Natl Acad Sci USA **109:** 19232–19237

Wu CC, Lin YC, Chen HT (2011) The TFIIF-like Rpc37/53 dimer lies at the center of a protein network to connect TFIIIC, Bdp1, and the RNA polymerase III active center. Mol Cell Biol **31:** 2715–2728

Xiu Z, Sun F, Shen Y, Zhang X, Jiang R, Bonnard G, Zhang J, Tan BC (2016) EMPTY PERICARP16 is required for mitochondrial nad2 intron 4 cis-splicing, complex I assembly and seed development in maize. Plant J **85:** 507–519

Yang J, Fu M, Ji C, Huang Y, Wu Y (2018) Maize oxalyl-CoA decarboxylase1 degrades oxalate and affects the seed metabolome and nutritional quality. Plant Cell **30:** 2447–2462

Yee NS, Gong W, Huang Y, Lorent K, Dolan AC, Maraia RJ, Pack M (2007) Mutation of RNA Pol III subunit rpc2/polr3b leads to deficiency of Subunit Rpc11 and disrupts zebrafish digestive development. PLoS Biol **5:** e312

Yi B, Zeng F, Lei S, Chen Y, Yao X, Zhu Y, Wen J, Shen J, Ma C, Tu J, et al (2010) Two duplicate CYP704B1-homologous genes BnMs1 and BnMs2 are required for pollen exine formation and tapetal development in *Brassica napus*. Plant J **63:** 925–938

Yi G, Neelakandan AK, Gontarek BC, Vollbrecht E, Becraft PW (2015) The naked endosperm genes encode duplicate INDETERMINATE domain transcription factors required for maize endosperm cell patterning and differentiation. Plant Physiol **167:** 443–456

Yoo SD, Cho YH, Sheen J (2007) Arabidopsis mesophyll protoplasts: A versatile cell system for transient gene expression analysis. Nat Protoc **2:** 1565–1572

Zhan J, Thakare D, Ma C, Lloyd A, Nixon NM, Arakaki AM, Burnett WJ, Logan KO, Wang D, Wang X, et al (2015) RNA sequencing of laser-capture microdissected compartments of the maize kernel identifies regulatory modules associated with endosperm cell differentiation. Plant Cell **27:** 513–531

Zhang XO, Gingeras TR, Weng Z (2019) Genome-wide analysis of polymerase III-transcribed *Alu* elements suggests cell-type-specific enhancer function. Genome Res **29:** 1402–1414

Zhang Z, Zheng X, Yang J, Messing J, Wu Y (2016) Maize endosperm-specific transcription factors O2 and PBF network the regulation of protein and starch synthesis. Proc Natl Acad Sci USA **113:** 10842–10847